RevMexAA (Serie de Conferencias), **1**, 179-186 (1995)

COLLAPSE OF MAGNETIZED MOLECULAR CLOUD CORES: MODEL PREDICTIONS VERSUS OBSERVATIONS

Daniele Galli
Osservatorio Astrofisico di Arcetri, Largo E. Fermi 5, I-50125 Firenze, Italy

RESUMEN

Después de hacer un breve resumen de los elementos básicos que han llevado al conocimiento actual del papel de los campos magnéticos en las regiones de formación estelar, discutimos los resultados de cálculos MHD en dos dimensiones del colapso de núcleos moleculares magnetizados. Con el fin de comparar, realizamos una breve revisión de los efectos de la rotación en el colapso de una nube. Se pone una atención especial en las implicaciones observacionales de los modelos, analizando en detalle unos cuantos casos significativos. En particular:
(*a*) Enfatizamos la importancia que tienen las observaciones del efecto Zeeman para obtener la geometría del campo magnético en las regiones de formación estelar;
(*b*) predecimos los signos cinemáticos del colapso más importantes observables a diferentes escalas alrededor de fuentes inmersas en la nube y de estrellas jóvenes;
(*c*) presentamos mapas sintéticos hechos en base a cálculos teóricos de la emisión continua en longitudes de onda milimétricas del polvo de envolturas contrayéndose;
(*d*) mostramos las simulaciones de Monte-Carlo para la intensidad/polarización de la luz dispersada en longitudes de onda del visible y cercano infrarrojo.

ABSTRACT

After a brief outline of the basic elements leading to our current understanding of the role of magnetic fields in star forming regions, we discuss the results of recent theoretical two-dimensional MHD calculations for the collapse of magnetized molecular cloud cores. For comparison, we briefly review the effects of rotation on cloud collapse. Special consideration is given to the observational implications of the models, and a few significant cases are analyzed in detail. In particular:
(*a*) we emphasize the relevance of Zeeman effect observations in order to derive the magnetic field geometry in star forming regions;
(*b*) we predict the relevant kinematical signatures of collapse observable on different spatial scales around embedded sources and young stars;
(*c*) we present synthetic maps computed on the basis of the theoretical calculations for the dust continuum emission at millimiter wavelengths of infalling envelopes.
(*d*) we show the results of Monte-Carlo simulations for the intensity/polarization of scattered light at optical and near-infrared wavelengths.

Key words: **ISM: CLOUDS — ISM: MAGNETIC FIELDS — MHD — STARS: FORMATION**

1. INTRODUCTION

From a theoretical viewpoint, it can be easily verified that the magnetic, gravitational and thermal energy of a typical molecular cloud core are of the same order of magnitude; clearly then, the magnetic field is destined to play a significant role in the evolution of a molecular cloud and in its eventual collapse.

We shall focus the attention here on the early phases of star formation, namely the anisotropic collapse of a molecular cloud core permeated by the local galactic magnetic field. We will examine qualitatively and

quantitatively the observational consequences of the theoretical scenario developed by Shu and coworkers (Terebey, Shu, & Cassen 1984; Lizano & Shu 1989; Galli & Shu 1993a,b) summarized in Sections 2 and 3. Then we will concentrate our discussion on:

(1) the magnetic field morphology in the collapse region (Section 4);

(2) the kinematic signatures of collapse (Section 5);

(3) the dust continuum emission in the far-infrared (Section 6); and

(4) the intensity and polarization of scattered light around young stars (Section 7).

2. THE EFFECTS OF MAGNETIC FIELDS

In a light ionized medium such as a the gas of a molecular cloud, the relevant mechanism of magnetic diffusion is the so-called *plasma drift* or *ambipolar diffusion*, a physical process originally investigated by Mestel & Spitzer (1956), in which the fluid of charged particles with its frozen-in magnetic field can slowly drift with respect to the fluid of neutral particles, the two fluids being collisionally coupled. Among others, Lizano & Shu (1989) have performed detailed ambipolar diffusion computations, including empirically the effects of turbulence, to follow the phase of formation of molecular cloud cores starting from an almost uniform initial configuration. Their study has shown that during the phase of quasistatic evolution molecular cloud cores tend to acquire the density profile of the singular isothermal sphere ($\rho \propto r^{-2}$), modified by a shape function accounting for the anisotropy of magnetic support. Their calculation was able to follow the *quasi-static* (i.e. driven by ambipolar diffusion) evolution of molecular cloud cores until they become gravitationally unstable in their central regions and undergo dynamical collapse. Lizano & Shu (1989) speculated that the resulting dynamical behavior would closely resemble the self-similar collapse solution found by Shu (1977).

Subsequently, as a natural continuation of the study by Lizano & Shu (1989), Galli & Shu (1993a,b) have performed two-dimensional MHD calculations (partly semi–analytically, partly numerically) to follow the dynamical collapse of a molecular cloud core, examining in detail the effects of the magnetic field and plasma drift to the original collapse solution of Shu (1977). As in that case, the collapse takes place in an inside-out fashion, propagating outward as a fast magnetosonic wave, traveling faster in the direction parallel to the initial magnetic field. One of the findings of this study is that the rate of mass accretion resulting from the collapse of the non-magnetic singular isothermal sphere is *not* significantly altered by the presence of the magnetic field: the gas falls inward slower than in the non-magnetic case, because of the Lorentz force opposing gravity, whereas the information travels outwards faster, because of the increased characteristic speed of the system. An important effect of the magnetic field on the collapse dynamics is the resulting Lorentz force that deflects infalling fluid elements toward the equatorial plane forming an inner disequilibrium structure (*pseudo-disk*) around the central protostar (see also the poster by Nakamura et al. at this Conference for a similar calculation in a different geometry). The size of the pseudo-disk can be characterized by a radius r_B defined as the radius inside which infalling fluid elements land on the equatorial plane:

$$r_B \simeq 600 \left(\frac{B_0}{30\ \mu\mathrm{G}}\right)^{4/3} \left(\frac{a_{\mathrm{eff}}}{0.35\ \mathrm{km\ s^{-1}}}\right)^{-1/3} \left(\frac{t}{10^5\ \mathrm{yr}}\right)^{7/3} \mathrm{AU},$$

where a_{eff} is the effective sound speed in the cloud and B_0 is the strength of the initial magnetic field.

3. THE EFFECTS OF ROTATION

Besides magnetic fields, any realistic calculation of the collapse of a molecular cloud core should include the effects of rotation. In fact, small but detectable level of rotation have been measured in the outer parts of molecular cloud cores (see, e.g, Goodman et al. 1993), whose dynamical importance is expected to increase during the collapse of the cloud, leading eventually to the formation of a centrifugally supported circumstellar disk.

A major theoretical contribution was provided by Terebey, Shu, & Cassen (1984), who formulated and solved in a semi-analytical way the problem of the collapse of a slowly rotating molecular cloud core as a perturbation to the non-rotating collapse of the singular isothermal sphere. As in the case of magnetic collapse,

no significant departure from the standard accretion rate was found, although the centrifugal force introduces deviations from the radial collapse on a scale characterized by a *centrifugal* radius

$$r_C \simeq 44 \left(\frac{a_{\rm eff}}{0.35 \text{ km s}^{-1}}\right) \left(\frac{\Omega_0}{10^{-13} \text{ s}^{-1}}\right)^2 \left(\frac{t}{10^5 \text{ yr}}\right)^3 \text{ AU},$$

where Ω_0 is the initial angular velocity of the core. Inside r_C, infalling matter on ballistic trajectories encounters a centrifugal barrier in the equatorial plane (if it conserves its initial specific angular momentum) and accumulates in a disk.

Depending on the conditions in the molecular cloud core, the pseudo-disk is larger than the centrifugal disk by about one or two orders of magnitude. Over scales of $\sim 10^3$ AU the dynamics of the infalling matter is dominated by magnetic and gravitational forces, and the density distribution is shaped in a disk-like structure. Over scales of $\sim 10^2$ AU, the dynamics of collapse is dominated by magnetic, gravitational and centrifugal forces.

Clearly, the next logical step would be to elaborate collapse models including the combined effects of rotation and magnetic fields. In addition, a more physical approach to the treatment of interstellar turbulence and its dynamical role would be desirable.

4. MAGNETIC FIELD STRUCTURE IN STAR FORMING CORES

Zeeman effect observations provide the only way to measure the component of the magnetic field strength along the line-of-sight ($\mathbf{B}_{\rm los}$) in dense and diffuse molecular clouds. In addition to classical single-dish Zeeman measurements, interferometric techniques make possible to map $\mathbf{B}_{\rm los}$ over a considerable fraction of a molecular cloud (Crutcher 1994). The region of massive star formation W3 in the Perseus arm offers a particularly remarkable example. Zeeman effect observations reveal a *reversal* of $\mathbf{B}_{\rm los}$ across the W3 core in the photodissociated but otherwise undisturbed gas surrounding the infrared source IRS 5 (Troland et al. 1989, Roberts et al. 1993), suggestive of a pinched hourglass morphology produced by gravitational collapse.

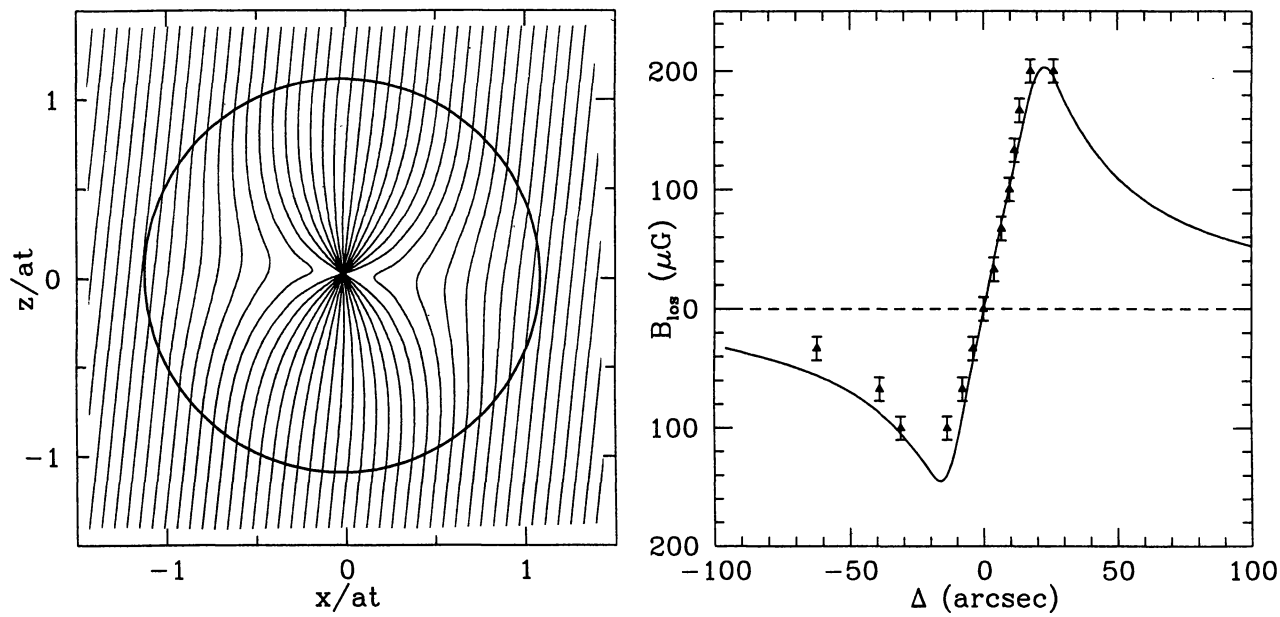

Fig. 1.— (a) Magnetic field lines during the collapse of the singular isothermal sphere, in the kinematic approximation. The thick circle represents the head of the expansion wave. — (b) Solid curve: theoretical profile of $\mathbf{B}_{\rm los}$ along the y-direction, averaged and convolved with the beam. Vertical bars: values of $\mathbf{B}_{\rm los}$ measured by Roberts et al. (1993) (see text for details).

We have modelled the field structure in W3 by using a simple model of magnetic collapse in the kinematic approximation (Galli & Shu 1993a): a singular isothermal sphere permeated by an initially uniform magnetic field (inclined by an angle ϕ to the line-of-sight) collapsing radially in the inside-out fashion computed by Shu (1977), kinematically dragging in the magnetic field lines. Despite the extreme oversimplication of the model, compared with the evident complexity of the W3 region, it is worth to examine the simplest case first. The model magnetic field is shown in Fig. 1a, in self-similar coordinates. By taking the average of the field component along the line-of-sight in the front half of the collapsing region (the other half of the region behind the protostar is not accessible to Zeeman measurements in HI absorption), and convolving the result with the synthesized beam used in the observations (25″), we obtain the curve shown in Fig. 1b. Vertical bars represent the reversal of $\mathbf{B}_{\rm los}$ as measured by Roberts et al. (1993) along the direction joining the positive and negative peaks of the magnetic field strength. The adjustable fit parameters are only two: the inclination angle $\phi = 4°$ and the initial total field strength $B_0 = 80$ μG (the latter being a scale factor for the theoretical curve). In addition, by assuming a distance $D = 1.8$ kpc (Ogura & Ishida 1976) and a sound speed in the gas $a = 0.2$ km s^{-1} (Dickel et al. 1980), it is possible to derive the predicted collapsed mass at the center, $M_* = 28(D/1.8\ {\rm kpc})(a/0.2\ {\rm km\ s^{-1}})^2\ M_\odot$. This value is not inconsistent with observations: from the estimated bolometric luminosity of IRS 5, $L_{\rm bol} \simeq 2 \times 10^5 L_\odot$ (Werner et al. 1980), we derive a stellar mass $M_* \simeq 30 M_\odot$ (on the ZAMS). Finally, it is worth noticing that the polarization of dust emission measured by Greaves, Murray, & Holland (1994) at 800 μm in several positions around IRS 5 is fully consistent with magnetic field lines that converge on the infrared source.

5. KINEMATIC SIGNATURES OF COLLAPSE

Observational evidence for large ($\sim 10^3$ AU) flattened distributions of gas around YSOs stellar objects has steadily accumulated during the past two decades (see e.g. Edwards et al. 1993 for a review). In most cases, observers have attempted to interpret their findings in terms of centrifugally-supported accretion disks even though the radial (or vertical) extent of the structures in some cases exceeds theoretical and dynamical expectations by one or two orders of magnitude. It is interesting to investigate whether pseudo-disks can account for the observed disk-like density structures mapped in molecular line emission around a few YSOs.

According to the theoretical scenario outlined in Sections 2 and 3, the dynamics of the gas undergoing dynamical accretion toward the central protostar/inner disk is dominated by the deflecting effects of the Lorentz force in a meridional plane containing the magnetic field and the protostar. Roughly speaking, then, *infalling* motions would dominate at intermediate radii (say from a few 10^2 to a few 10^3 AU), whereas *rotational* motions would prevail in the inner region of collapse (say, inside a few 10^2 AU).

Detection of dynamically accreting disks around both optically revealed stars and embedded sources represents a major step toward a complete understanding of the physical processes at work during the collapse of a molecular cloud core (a noticeable example is presented in the poster by Liljeström & Olofsson, at this Conference). Although a rather robust spectroscopic evidence of infall has been found in several low-mass star forming regions (Zhou et al. 1990, Zhou 1992), *direct* observational evidence of dynamical collapse is still rather sparse. Perhaps the only object where the case for accretion is convincingly supported by observations of the gas kinematics is the T Tauri star HL Tau. Observations of the ^{13}CO emission around this source carried out with the Nobeyama Millimeter Array (Hayashi et al. 1993) have revealed that the velocity gradients in the flattened structure (radius $\sim 2 \times 10^2$ AU) associated with HL Tau mostly lie along the minor axis rather than along the major axis, consistently with the velocity field expected for a pseudo-disk (magnetically diluted infall), rather than with that of a rotating disk (see, however, the poster presented by Cabrit et al. at this Conference for a different interpretation). A more quantitative test of the model will be given by radiative transfer calculations of line profiles from pseudo-disks that are currently in progress (van der Tak & van Langevelde, priv. comm.).

6. FAR-INFRARED EMISSION OF PSEUDO-DISKS

Since pseudo-disks are dense, extended, infalling envelopes of gas and dust, they will contribute significantly to the continuum emission measured in protostellar environments. To evaluate this contribution, we have computed (Ménard & Galli, in preparation) the intensity of the millimeter continuum radiation emitted by thermal dust grains heated at a constant temperature T_d and distributed according to the MHD collapse model by Galli & Shu (1993a,b).

For optically thin emission (a valid approximation at millimeter wavelengths), the specific intensity is

$$I_\nu(b) = \int_{-\infty}^{+\infty} B_\nu(T_d)\rho\kappa_\nu d\ell,$$

where b is the impact parameter in the plane of sky, ρ is the gas density, κ_ν is the gas opacity, and $B_\nu(T_d)$ is the Planck function. We have expressed the opacity at millimeter wavelengths as a power law,

$$\kappa_\nu = \kappa_0 \left(\frac{\lambda_0}{\lambda}\right)^\beta,$$

assuming the fiducial values $\kappa_0 = 0.1$ cm^2 g^{-1} at $\lambda_0 = 0.025$ cm and $\beta = 1.5$ (Terebey, Chandler, & André 1993). The integrated flux density within an angular radius θ is then

$$S_\nu(\theta) = \int_0^{\theta D} I_\nu(b)\frac{2\pi b}{D^2} db,$$

where D is the distance to the source. The peak flux $S_\nu^{\rm peak}$ measured with a telescope of beamsize $2\theta_b$ is given by the expression above with $\theta = \theta_b$. In our computations we have assumed a beam of angular size $2\theta = 11''$ (IRAM) and a distance $D = 160$ pc (ρ-Ophiuchi).

For the initial configuration, a singular isothermal sphere with density distribution $\rho(r) = a_{\rm eff}^2/2\pi G r^2$, the calculation outlined above gives the peak millimetric flux

$$S_\nu^{\rm peak} = 240 \left(\frac{\lambda}{1.3\ {\rm mm}}\right)^{-3.5} \left(\frac{T_d}{30\ K}\right) \left(\frac{a_{\rm eff}}{0.35\ {\rm km\ s^{-1}}}\right)^2 \left(\frac{D}{160\ {\rm pc}}\right)^{-1} \left(\frac{2\theta_b}{11''}\right) \quad {\rm mJy\ beam^{-1}},$$

well above the sensitivity threshold of the IRAM telescope. This value can be regarded as an upper limit to the continuum emission at any subsequent stage. In fact, after the onset of collapse the dust mass in the envelope

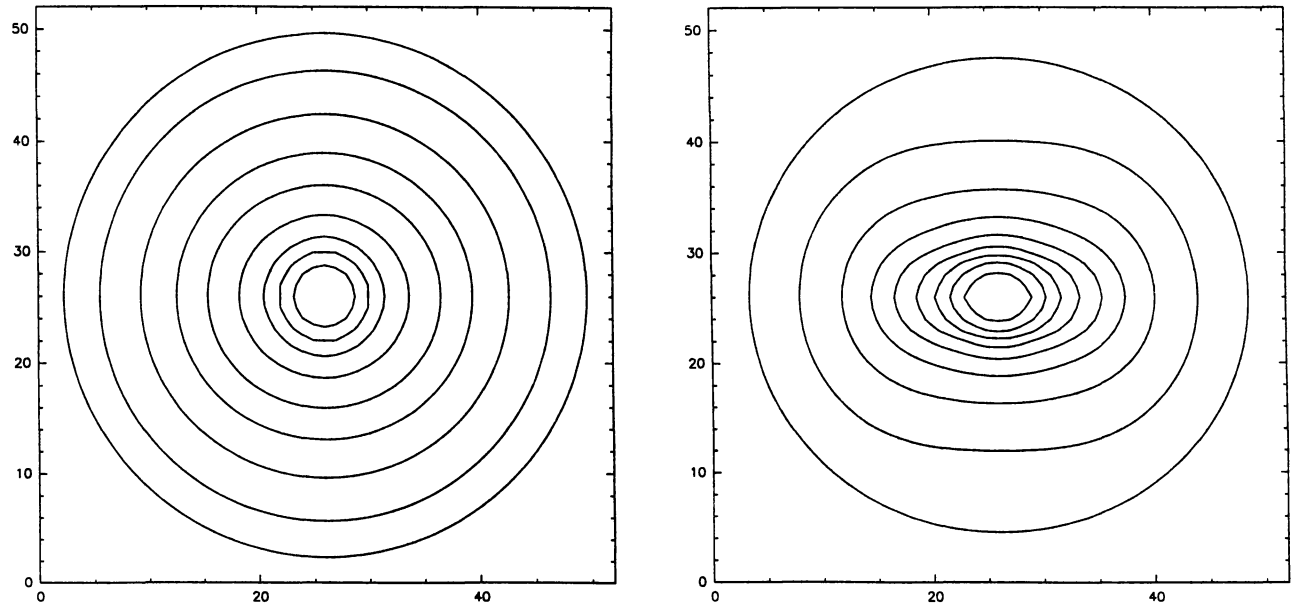

Fig. 2 — Synthetic millimeter continuum maps for a pseudo-disk at $t = 2 \times 10^5$ yr, observed pole-on (a) and edge-on (b). Contour levels range from 0.1 to 0.9 of the peak value in steps of 0.1. At 1.3 mm, the peak values are 25 mJy for the pole-on case and 34 mJy for the edge-on case.

decreases with time, about one half of the mass originally enclosed inside the expansion wave having been accreted on the central protostar at each time. Consequently, the continuum emission steadily decreases. After a time $t = 8.6 \times 10^4$ yr from the onset of collapse the peak value at 1.3 mm is $S_\nu^{\rm peak} = 54$ mJy; at $t = 2 \times 10^5$ yr, $S_\nu^{\rm peak} = 25$ mJy. Thus, younger sources, with larger envelope masses (and lower protostellar masses) should have higher continuum emission. These predicted values, although affected by the uncertainty on the opacity law at millimetric wavelengths, are consistent with observations. In particular, this model can account for most of the observed single-dish emission at 1.3 mm of ρ-Ophiuchi sources reported by André & Montmerle (1994); a few sources show spatially resolved structure, and one has an elongated shape suggestive of an edge-on pseudo-disk. However the emission from Class 0 sources is generally too high to be explained by this model.

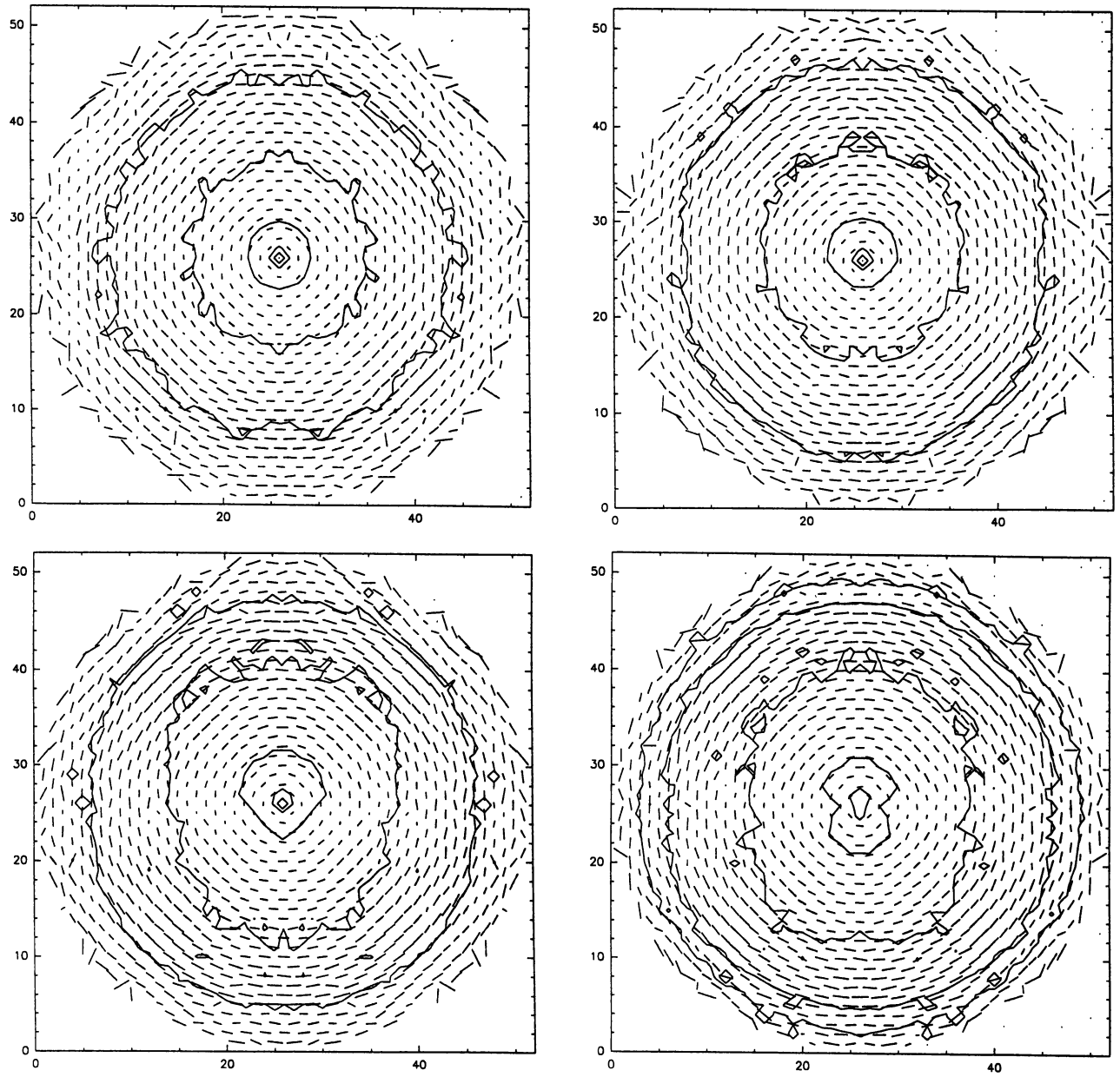

Fig. 3 — Intensity and polarization maps for a pseudo-disk at $t = 2 \times 10^5$ yr in the I-band at different viewing angles (17°, 51°, 69°, and 89°).

7. NEAR-INFRARED INTENSITY AND POLARIZATION MAPS OF PSEUDO-DISKS

At near-infrared wavelengths (1–2.2 μm), the light distribution around YSOs results from scattering (and absorption) by circumstellar dust of the radiation emitted by the central source. An increasing amount of observational data in this wavelength range seems to suggest the presence of large (size $\sim 10^3$ AU) dusty "disks" as well as of bipolar "cavities" in the gas surrounding the central source (see, e.g., Staude & Elsässer 1993 for a review; a remarkable object of this class was described in the poster by Boulard et al. at this Conference).

Another tool that has proven especially valuable for the theoretical interpretation of the origin of extended structures around YSOs comes from the existence of fractional polarizations in the light from some angularly unresolved YSOs and in the associated reflection nebulae. Polarization maps of circumstellar regions around YSOs often show a centro-symmetric pattern of polarization vectors at the peripheries (the expected signature of single scattering of starlight) and a more puzzling elliptical or even linear alignment of polarization vectors closer to the central source (the so called "polarization disk"). The interpretation of the latter feature is still controversial (Gething et al. 1982; Bastien & Ménard 1988; Gledhill 1991), but in a way or another probably requires the presence of a disk-like density distribution.

Here we present Monte-Carlo simulations of intensity and polarization maps (Ménard & Galli, in preparation) for the MHD collapse model of Galli & Shu (1993a,b). Using spherical silicate grains of radius $a = 0.1$ μm (optical constants from Draine & Lee 1984), we calculated intensity/polarization maps in the V, I, J, and K bands at 10 angles of inclination and for three timesteps of evolution ($t = 0.86 \times 10^5$ yr, $t = 1.43 \times 10^5$ yr and $t = 2 \times 10^5$ yr), using the Monte-Carlo code originally developed by Ménard (1989).

Some results are shown in Fig. 3. Each side of the maps corresponds to 2×10^4 AU (= 133″ at a distance of 150 pc). The computed maps show typical characteristics observed in reflection nebulae around YSOs, the prominent one being the centro-symmetric pattern of polarization vectors and the pinching of the isophotes in the edge-on maps (more conspicuous at shorter wavelengths). The latter feature outlines the contour of the optically thick part of the pseudo-disk. A "monopolar" shape of the isophotes is also apparent in a few cases at intermediate inclinations. It is also evident that the peak of the infrared emission can be significantly displaced from the true stellar position (at the center of the map).

In the maps shown here, no region of aligned vectors is produced. Rather, the density distribution of the pseudo-disk produces an overall depolarization of the scattered starlight close to the central source. A full exploration of the parameter space aimed at determining the physical conditions required to obtain a pattern of aligned vectors is currently in progress (Ménard & Galli, in preparation).

REFERENCES

André, P. & Montmerle, T. 1994, ApJ, 420, 837
Bastien, P., & Ménard, F. 1988, ApJ, 326, 334
Bastien, P., 1991, in The Physics of Star Formation & Early Stellar Evolution, ed. C.J. Lada & N. Kylafis (Dordrecht: Kluwer), 709
Crutcher, R. M. 1994, in Clouds, Cores & Low Mas Stars, ed. D.P. Clemens & R. Barvainis, ASP Conf. Ser., 95, 87
Dickel, H. R., Dickel, J. R., Wilson, W. J., & Werner, M. W. 1980, ApJ, 237, 711
Draine, B. T., & Lee, H. M. 1984, ApJ, 285, 89
Edwards, S., Ray, T., & Mundt, R. 1993, in Protostars & Planets III, ed. M.S. Mathews & E. Levy (Tucson: University of Arizona Press)
Galli, D., & Shu, F. H. 1993a, ApJ, 417, 220
Galli, D., & Shu, F. H. 1993b, ApJ, 417, 243
Gething, M. R., Warren-Smith, R. F., Scarrott, S. M., & Bingham R. G. 1982, MNRAS, 198, 881
Goodman, A. A., Benson, P. J., Fuller, G. A., & Myers, P. C. 1993, ApJ, 406, 508
Hayashi, M., Ohashi, N., & Miyama, S. M. 1993, ApJ, 418, L71
Lizano, S., & Shu, F. H. 1989, ApJ, 342, 834
Ménard, F. 1989, Ph. D. Thesis, University of Montréal
Mestel, L., & Spitzer, L. 1956, MNRAS, 212, 275
Ogura, K., & Ishida, K. 1976, PASJ, 28, 651
Roberts, D. A., Crutcher, R. M., Troland, T. H., & Goss, W. M. 1993, ApJ, 412, 675
Shu, F. H. 1977, ApJ, 214, 488
Staude, H. J., & Elsässer, H. 1993, A&AR, 5, 165
Terebey, S., Shu, F. H., & Cassen, P. C. 1984, ApJ, 286, 529

Terebey, S., Chandler, C. J., & André, P. 1993, ApJ, 414, 759
Troland, T. H., Crutcher, R. M., Goss, W. M., & Heiles, C. 1989, ApJ, 347, L89
Ward-Thompson, D., Warren-Smith, R. F., Scarrott, S. M., & Wolstencroft, R. D. 1985, MNRAS, 215, 537
Warren-Smith, R. F., Draper, P. V., & Scarrott, S. M., 1987, MNRAS, 227, 749
Werner, M. W., Becklin, E. E., Gatley, I., Neugebauer, G., Sellgren, K., Thronson, H. A., Harper, D. A., Lowenstein, R., & Moseley, S. H. 1980, ApJ, 242, 601
Zhou, S., Evans, N. J., Butner, H. M., Kutner, M. L., Leung, C. M, & Mundy, L. G. 1990, ApJ, 363, 168
Zhou, S. 1992, ApJ, 394, 204